This is the peer reviewd version of the followng article:

Design-oriented modelling of composite actuators with embedded shape memory alloy / Mizzi, Luke; Spaggiari, Andrea; Dragoni, Eugenio. - In: COMPOSITE STRUCTURES. - ISSN 0263-8223. - 213:(2019), pp. 37-46. [10.1016/j.compstruct.2019.01.057]

Terms of use:

The terms and conditions for the reuse of this version of the manuscript are specified in the publishing policy. For all terms of use and more information see the publisher's website.

16/05/2026 19:38

(Article begins on next page)

Accepted Manuscript

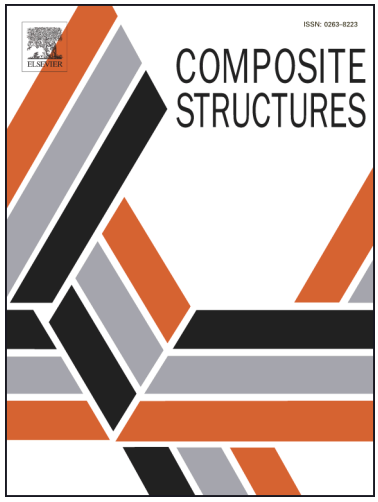

Design-oriented modelling of Composite Actuators with embedded Shape Memory Alloy

Luke Mizzi, Andrea Spaggiari, Eugenio Dragoni

PII: S0263-8223(18)33454-8
DOI: https://doi.org/10.1016/j.compstruct.2019.01.057
Reference: COST 10574

To appear in: *Composite Structures*

Received Date: 13 September 2018
Revised Date: 3 December 2018
Accepted Date: 11 January 2019

Please cite this article as: Mizzi, L., Spaggiari, A., Dragoni, E., Design-oriented modelling of Composite Actuators with embedded Shape Memory Alloy, *Composite Structures* (2019), doi: https://doi.org/10.1016/j.compstruct.2019.01.057

This is a PDF file of an unedited manuscript that has been accepted for publication. As a service to our customers we are providing this early version of the manuscript. The manuscript will undergo copyediting, typesetting, and review of the resulting proof before it is published in its final form. Please note that during the production process errors may be discovered which could affect the content, and all legal disclaimers that apply to the journal pertain.

ACCEPTED MANUSCRIPT

Design-oriented modelling of Composite Actuators with embedded Shape Memory Alloy

Luke Mizzi[1*], Andrea Spaggiari[1], Eugenio Dragoni[1]

[1]*Dipartimento di Scienze e Metodi dell'Ingegneria, Università di Modena e Reggio Emilia*

**corresponding author: luke.mizzi@unimore.it*

Abstract

Shape memory alloy (SMA) actuators have generated a great deal of interest in recent years due to their reusability and ability to exhibit a wide spectrum of actuation properties. In this work we present an analytical approach through which one may predict the actuation stroke as well as recovery potential of a two-component SMA-based composite actuator. The predictions of the analytical model were validated using Finite Element (FE) simulations on a composite SMA actuator designed in the form of an SMA strip embedded within an elastic matrix, where the shape memory effect of the SMA component was modelled using the numerical Souza-Auricchio model. The results obtained from the two approaches show extremely good agreement. The trends found upon altering various geometric and material parameters within the system provide a thorough understanding of how one can vary these parameters in order to obtain a tailored actuation and recovery response from the SMA-based actuator.

Keywords: Shape Memory Alloys, Actuators, Composites, Analytical Modelling, Finite Element Analysis.

Nomenclature:

F	Force
d	Displacement
F_i	Applied force due to initial pre-stretch
d_i	Applied initial pre-stretch
k_M	Stiffness of twinned martensitic state of SMA component
k_T	Stiffness of transition phase of SMA component
k_{DM}	Stiffness of detwinned martensitic state of SMA component
F_T	Force threshold required to transform from twinned martensite to transition phase
d_T	Displacement threshold required to transform from twinned martensite to transition phase
F_{DM}	Force threshold required to transform from transition phase to fully detwinned martensite
d_{DM}	Displacement threshold required to transform from transition phase to fully detwinned martensite
k_A	Stiffness of the linear austenitic phase of SMA component
k_{CB}	Stiffness of counterbalance component
$F_{EQ,C1}$	Initial cold state equilibrium force between SMA component and counterbalance
$d_{EQ,C1}$	Initial cold state equilibrium displacement between SMA component and counterbalance
$F_{EQ,H}$	Hot state equilibrium force between SMA component and counterbalance
$d_{EQ,H}$	Hot state equilibrium displacement between SMA component and counterbalance
$F_{EQ,C2}$	Recooling cold state equilibrium force between SMA component and counterbalance
$d_{EQ,C2}$	Recooling cold state equilibrium displacement between SMA component and counterbalance
m	Slope factor relating d_i with (d_T, F_T)
F_A	Morphing Force
d_A	Actuation Stroke (Displacement)
F_R	Recovery Force
d_R	Recovery Stroke (Displacement)
l_0	Initial length of SMA composite system before the application of pre-stretch
h_{Matrix}	Length of matrix counterbalance component

ACCEPTED MANUSCRIPT

E_{Matrix}	Young's Modulus of matrix counterbalance component
v_{Matrix}	Poisson's Ratio of matrix counterbalance component
h_{SMA}	Length of SMA component
v_{SMA}	Poisson's Ratio of SMA component
E_A	Young's Modulus of initial linear austenitic state of SMA
E_M	Young's Modulus of twinned martensitic SMA
E_{DM}	Young's Modulus of detwinned martensitic SMA
H	Hardening parameter
R	Elastic limit
e_L	Maximum transformation strain
T_0	Reference conversion temperature
β	Temperature scaling parameter
ε_i	Applied pre- strain
T_f	Final temperature following heating of SMA component
ε_T	Strain threshold required to transform from twinned martensite to transition phase
σ_T	Stress threshold required to transform from twinned martensite to transition phase
ε_{DM}	Strain threshold required to transform from transition phase to fully detwinned martensite
σ_{DM}	Stress threshold required to transform from transition phase to fully detwinned martensite
$\varepsilon_{EQ,C1}$	Initial cold state equilibrium strain between SMA component and counterbalance
$\varepsilon_{EQ,H}$	Hot state equilibrium strain between SMA component and counterbalance
$\varepsilon_{EQ,C2}$	Recooling cold state equilibrium strain between SMA component and counterbalance
T_{Trans}	Phase Transformation Temperature

1. Introduction

Shape memory alloys (SMAs) are materials that 'remember' their shape after loading and return to their original conformation after heating [1–5]. This effect comes about due to a phase transition from the cold martensitic phase to the hot austenitic phase and makes these materials ideal for a number of applications [6] such as stents [7–10], sensors [11,12] and sports apparel including golf clubs [13,14]. SMAs have also been implemented in composite structures in order to enhance the functionality of such systems [15–17]. Another field in which SMAs have generated a great deal of interest is that of actuation. SMA-based actuators have the potential to exhibit a wide range of actuation properties ranging from high force/low stroke ratios for SMA wires to low force/high stroke ratios for SMA spring-based systems [18–21]. Typical SMA actuators are designed as two component systems incorporating an agonist-antagonistic relationship. The counterbalance effect provided by the additional component to the system besides the SMA part may come about in various forms, including a fixed load, an elastic material or even an opposing SMA system, and its main function is to impart reusability to the SMA actuator [22–28].

One method to produce such two-component SMA actuators is by embedding SMA wires in a matrix [29–32]. This technique involves stretching an SMA wire and forming a matrix by pouring the uncured resin around the pinned, stretched wire. Once the resin cures and the matrix is formed, the wire is released and the system equilibrates at a fixed displacement point, provided that there is a good level of adhesion between the matrix and the wire. One may obtain an actuation effect from this composite system by heating the wire. Then, once the system is cooled, the matrix, which acts as a counterbalance to the SMA wire, forces the actuator to return to its original equilibrium point, hence reversing the contraction of the wire and making the actuator reusable.

The efficacy of an SMA composite actuator is dependent primarily on the relative stiffnesses of the counterbalance and the SMA component [26,28]. If the counterbalance component is too

ACCEPTED MANUSCRIPT

stiff, then the SMA component will not be able to return to its original size when heated. On the other hand, if the counterbalance is too soft, it will not be able to reverse the actuation of the SMA component, rendering the actuator unsuitable for multiple usage. These problems highlight the delicate balance which one must consider when designing a SMA composite actuator.

In view of this, in this work, we present a method through which one may design and optimize the geometry of an SMA composite actuator in order to obtain a tailored stroke based on the individual force-displacement curves of the SMA and counterbalance components of the system. An analytical model which can predict the actuation output and recovery of the actuator was derived and validated using Finite Element (FE) simulations. This model is expected to facilitate the pre-design of SMA composite actuators by quantifying the relationship between the material properties of the individual components of the composite and the geometric parameters of the system. This model also improves on previous models found currently in literature [22,33] by considering the recovery potential of the actuator and by considering the force-displacement behaviour of the martensitic SMA in terms of three distinct regions rather than as one linear model.

2. Theoretical Approach

The model presented in this work is based on a two-component actuator system made up of an SMA and a counterbalance force. The model presented here is unidimensional, i.e. it considers only uniaxial tensile and compressive deformations and the actuator is assumed to be produced by the same principles described for the SMA wire/matrix composite actuator mentioned previously [29]. Broadly, this means that first the martensite SMA component is pre-stretched and then the counterbalance component is added and the system is allowed to reach its equilibrium point. Then the SMA component is heated to obtain an actuation effect, followed by re-cooling in order to recover the actuation stroke. A schematic of this process is presented in **Figure 1**.

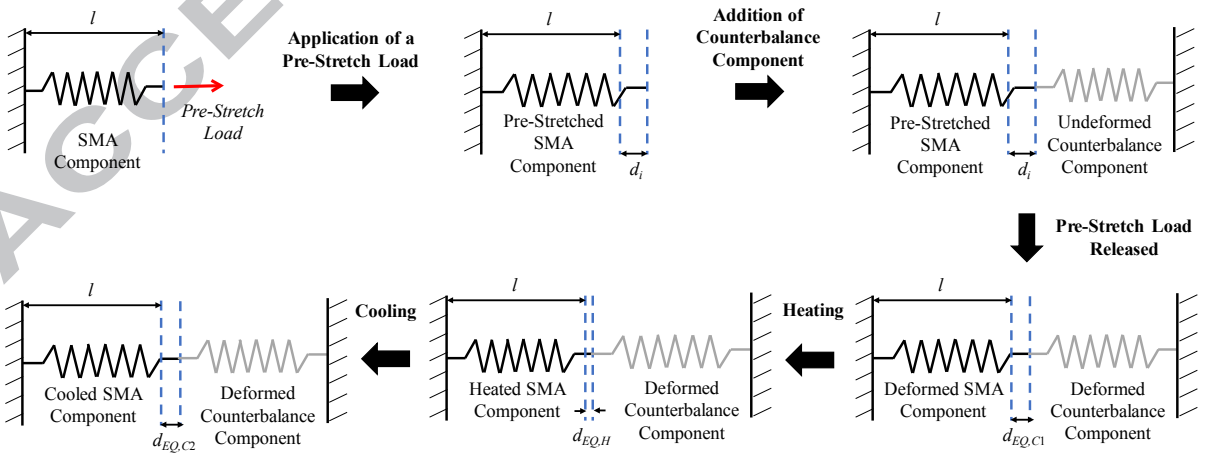

Figure 1: A schematic of the construction and function of a generalized two component SMA actuator.

As shown in **Figure 1**, the system has three equilibration point displacements: $d_{EQ,C1}$, $d_{EQ,H}$, and $d_{EQ,C2}$, where the first is the equilibrium point of the cold pre-stretched SMA component and the counterbalance component, the second, the equilibrium point of the heated SMA

ACCEPTED MANUSCRIPT

component and counterbalance and the last, that of the cooled SMA component and the counterbalance. At each of these equilibrium points, the force exerted by the SMA component must be equal to the opposing force imparted by the counterbalance component of the system. This means that through force-displacement plots of the two separate components such as the one shown in **Figure 2a**, one may be able to predict the exact displacements at which equilibrium is achieved in each of the three cases.

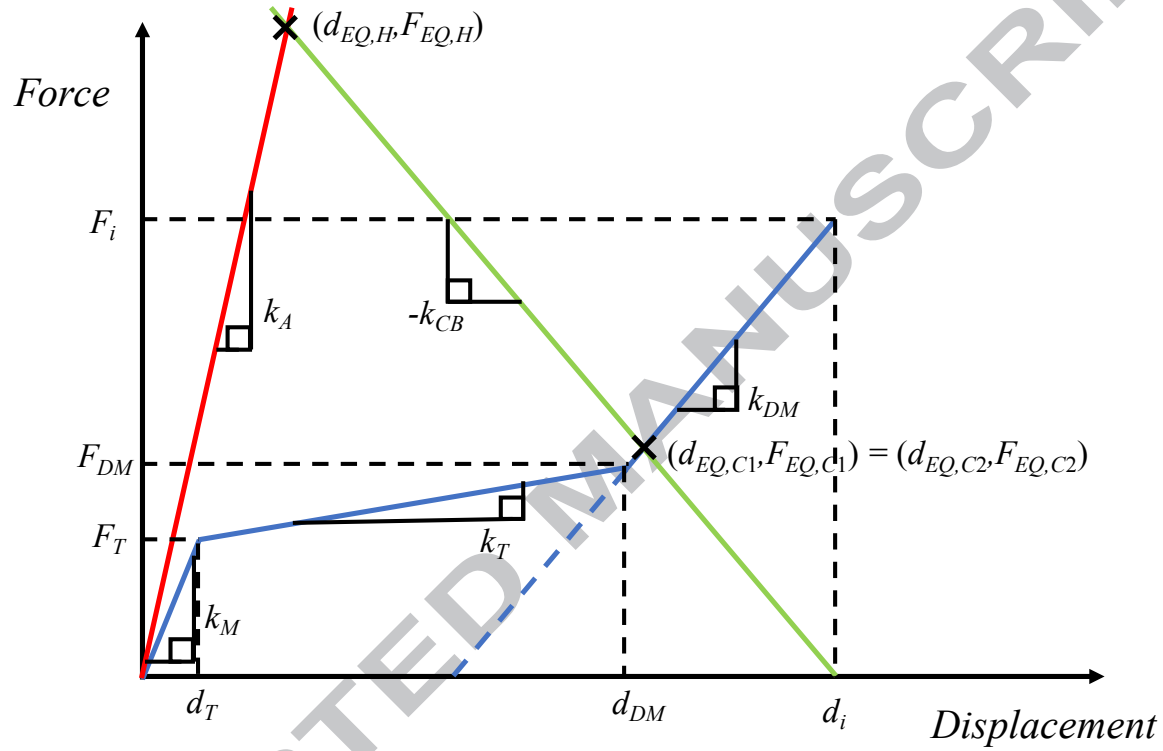

Figure 2: A qualitative force-displacement plot of an SMA actuator showing the separate plots of the components making up the system. The blue line represents the force-displacement behaviour of the cold martensitic SMA component, the red line the hot austenitic SMA and the green line the behaviour of the counterbalance, which in this case is represented as a linear elastic deformation behaviour.

Figure 2 shows a qualitative example of a force-displacement of the components making up an SMA actuator. The blue line represents an idealised typical material martensitic SMA force-displacement relationship, which may be represented by three linear plots each of which depict the different deformation behaviour observed in the three distinct regions shown in **Figure 2**. The first region represents the linear elastic deformation of twinned martensitic SMA and has a stiffness of k_M. The second is the transition phase from twinned martensitic SMA to detwinned martensitic SMA and is usually marked by a relatively low stiffness value in comparison to the initial linear region of deformation, is denoted by the stiffness value k_T. The third region, which has a stiffness of k_{DM}, represents the detwinned martensite phase of the SMA component. The transition points between these regions are indicated by (d_T, F_T) and (d_{DM}, F_{DM}) as shown in **Figure 2**. On the other hand, the red line represents the linear elastic region of deformation of the hot austenitic SMA component and has a stiffness value of k_A. In the case presented here, for the sake of simplicity, the counterbalance component is depicted

ACCEPTED MANUSCRIPT

in the form of a linear elastic system with a constant stiffness value of k_{CB}. However, it is important to note that in reality any force-displacement plot may be used to depict the elongation of the counterbalance component upon loading and that the method presented here is not limited solely to a linear model.

As shown in **Figure 2**, at a cold temperature, the equilibration point of the system may be defined as the point where the force-displacement plot of the martensitic SMA meets that of the counterbalance, ($d_{EQ,C1}$, $F_{EQ,C1}$). Upon heating, if a complete conversion to austenite is assumed to be achieved, then the equilibrium point shifts to the point where the matrix plot crosses the linear region of the austenitic SMA force-displacement graph ($d_{EQ,H}$, $F_{EQ,H}$). The difference in displacement between the two points may be defined as the actuation stroke of the system, d_A, while the morphing force (or force required to achieve this displacement), F_A, is the difference in force between these two points. In the case shown in Figure 2, upon re-cooling the SMA back to its initial temperature, the equilibrium point shifts back to its original equilibrium point ($d_{EQ,C2}$, $F_{EQ,C2}$).

The three linear equations of the cold martensitic SMA component may be written in terms of k, F and d as follows:

$$F = k_M d \qquad \textbf{Eq. 1}$$

$$F = k_T d + F_T - k_T d_T \qquad \textbf{Eq. 2}$$

$$F = k_{DM} d + F_{DM} - k_{DM} d_{DM} \qquad \textbf{Eq. 3}$$

while for the austenitic SMA, the equation may be defined as:

$$F = k_A d \qquad \textbf{Eq. 4}$$

A similar term may also be used to describe the counterbalance force-displacement relationship, although the slope is negative in this case since the displacement of the counterbalance occurs in the opposite direction to that of the initial pre-stretch displacement, d_i.

$$F = -(k_{CB})d + k_{CB} d_i \qquad \textbf{Eq. 5}$$

These five equations may be obtained by fitting linear plots on the experimental force-displacement plots of martensitic SMA, austenitic SMA and the counterbalance component respectively. In order for the model to function properly, the fitting must return a positive slope, k, value for all equations from the force-displacement plots. For the counterbalance (**Eq. 9**), the fitting should return only the k_{CB} value (which is positive), which is then inserted into **Eq. 9**.

If the SMA component is applied a pre-stretch load which is higher than F_{DT}, then the equilibrium force at a cold temperature, $F_{EQ,C1}$, may be defined as the point where the force imparted by the counterbalance component is equal to that exerted by the detwinned martensite region, i.e. where **Eq. 5** is equal to **Eq. 3**. This assertion holds also for values where $F_{EQ,C1}$ is lower than F_{DT} since once the load is released, the SMA does not follow the same path, i.e. force-displacement curve, as loading when unloading, but rather follows the linear detwinned

ACCEPTED MANUSCRIPT

behaviour (indicated by the dashed blue line in **Figure 2**). At cold temperatures, the martensitic return may normally be defined in a linear manner by **Eq. 3**. Thus, the equilibrium cold force, $F_{EQ,C1}$, and displacement, $d_{EQ,C1}$, values may be found as follows:

$$F_{EQ,C1} = -\frac{k_{CB}(d_{DM}k_{DM} - d_i k_{DM} - F_{DM})}{k_{CB} + k_{DM}} \quad \textbf{Eq. 6}$$

$$d_{EQ,C1} = \frac{d_{DM}k_{DM} + d_i k_{CB} - F_{DM}}{k_{CB} + k_{DM}} \quad \textbf{Eq. 7}$$

Once the system is heated and complete austenite transformation is achieved, the equilibrium translates to the point where **Eq. 5** is equal to **Eq. 4**. Therefore, the equilibrium hot force, $F_{EQ,H}$, and displacement, $d_{EQ,H}$, values may be written as:

$$F_{EQ,H} = \frac{k_A k_{CB} d_i}{k_{CB} + k_A} \quad \textbf{Eq. 8}$$

$$d_{EQ,H} = \frac{k_{CB} d_i}{k_{CB} + k_A} \quad \textbf{Eq. 9}$$

The resultant actuation stroke, d_A, and morphing force, F_A, may be calculated from the differences between the two equilibrium points and may be defined as:

$$F_A = F_{EQ,H} - F_{EQ,C1} \quad \textbf{Eq. 10}$$

$$d_A = d_{EQ,C1} - d_{EQ,H} \quad \textbf{Eq. 11}$$

A similar approach is used in order to calculate the recovered force and displacement after the SMA is cooled back to its initial temperature. However, upon cooling, the system returns to its original equilibration point of $F_{EQ,C1}$ and $d_{EQ,C1}$ only if $F_{EQ,C1} > F_{DM}$. Otherwise the cooling equilibration point ($d_{EQ,C2}$, $F_{EQ,C2}$) will be either at the point where **Eq. 5** is equal to **Eq. 1** or the point where **Eq. 5** is equal to **Eq. 2**. In order to determine which pair of equations will yield the correct cooling equilibrium point, one must first find the force-displacement slope of the initial pre-stretch, d_i, relative to the first transition point of the martensitic SMA, (d_T, F_T). This value, denoted as m may be found as follows:

$$m = -\frac{F_T}{d_T - d_i} \quad \textbf{Eq. 12}$$

If $k_{CB} < m$, then the values for $F_{EQ,C2}$ and $d_{EQ,C2}$ may be quantified through:

$$F_{EQ,C2} = \frac{k_M k_{CB} d_i}{k_{CB} + k_M} \quad \textbf{Eq. 13}$$

$$d_{EQ,C2} = \frac{k_{CB} d_i}{k_{CB} + k_M} \quad \textbf{Eq. 14}$$

ACCEPTED MANUSCRIPT

However, if $k_{CB} > m$, such as in the example shown in **Figure 3a**, then the point ($d_{EQ,C2}$, $F_{EQ,C2}$) is equal to the solution of **Eq. 5** and **Eq. 2**, which may be found by:

$$F_{EQ,C2} = \frac{k_{CB}\left(d_i k_T + F_T - d_T k_T\right)}{k_{CB} + k_T} \qquad \textbf{Eq. 15}$$

$$d_{EQ,C2} = \frac{d_T k_T + d_i k_{CB} - F_T}{k_{CB} + k_T} \qquad \textbf{Eq. 16}$$

Finally, as stated previously, if, like the example shown in **Figure 2**, $F_{EQ,C1} > F_{DM}$, then $F_{EQ,C1} = F_{EQ,C2}$ and thus the whole actuation length and force is recovered completely. The magnitude of the recovered stroke, d_R, and force, F_R, may be calculated as follows:

$$F_R = F_{EQ,H} - F_{EQ,C2} \qquad \textbf{Eq. 17}$$

$$d_R = d_{EQ,C2} - d_{EQ,H} \qquad \textbf{Eq. 18}$$

The equations shown above may be used to calculate the actuation stroke and force of a system where the SMA component has been subjected to a pre-stress or pre-strain which results in a complete detwinned martensite transformation. While this is typically the case for SMA wires or strips, which usually undergo this transformation at relatively low strains, in cases of SMA springs or highly strained SMA wires which have a much longer transition phase, the initial pre-stretch applied to the SMA component may not be sufficient to reach the complete detwinning. An example of a force-displacement plot of such a system is shown in **Figure 3b**.

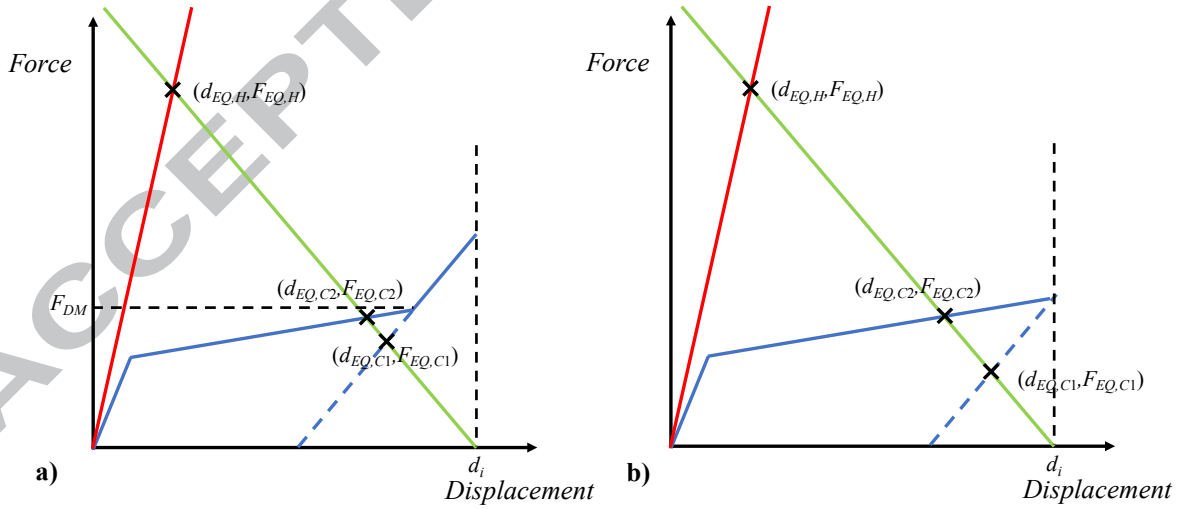

Figure 3: Force-displacement plots of a) a system which is pre-stretched up to the fully detwinned martensite region and has an initial equilibration force, $F_{EQ,C1}$, which is lower than F_{DM} and b) a system which is pre-stretched up to the transition phase only, i.e. $d_i < d_{DM}$. As in Figure 2, the red line represents the austenitic plot, the blue line the martensitic plot and the green the linear elastic counterbalance.

While the system has not reached the completed detwinned martensite phase, once the system is released from its initial pre-stretch, it still follows the slope of the detwinned martensite.

ACCEPTED MANUSCRIPT

Therefore, in order to find the initial cold equilibrium point, ($d_{EQ,C1}$, $F_{EQ,C1}$) for this scenario, the equation of the 'release' slope (see **Figure 3b**, the dotted blue line) which has the same gradient as the detwinned martensite slope, can be written as follows, instead of **Eq. 3**:

$$F = k_{DM} d - d_T k_T - d_i k_{DM} + d_i k_T + F_T \qquad \textbf{Eq. 19}$$

and the equilibrium point parameters may be found by solving **Eq. 19** and **Eq. 5**:

$$F_{EQ,C1} = \frac{k_{CB}\left(d_i k_T + F_T - d_T k_T\right)}{k_{CB} + k_{DM}} \qquad \textbf{Eq. 20}$$

$$d_{EQ,C1} = \frac{d_T k_T + d_i k_{DM} - d_i k_T + d_i k_{CB} - F_T}{k_{CB} + k_{DM}} \qquad \textbf{Eq. 21}$$

The terms for $F_{EQ,H}$, $d_{EQ,H}$, $F_{EQ,C2}$ and $d_{EQ,C2}$ remain unchanged for this case and thus the actuation and recovery stroke and force may be calculated using **Eq. 10**, **11**, **16** and **17** as in the previous case. A comprehensive analysis of the analytical expressions and all the individual cases described by **Eq. 1-21** is presented in the Supplementary Information. In addition, the micromechanical properties of the actuator at various equilibrium points are also presented here.

3. Finite Element Methodology

In order to validate the theoretical approach presented in the previous section, a series of Finite Element simulations were conducted on a range of SMA actuators using the ANSYS16 Multiphysics software. These actuators were designed in the form of an SMA wire/strip and matrix composite similar to those proposed by [29]. This means that the SMA component is confined between two layers of matrix which act as the linear elastic counterbalance of the system. In order to achieve maximal computational efficiency and to allow for comparison with the 1D analytical model, the systems were modelled as 2D 'half-systems' with mirror boundary conditions as shown in **Figure 4**. The thermo-structural PLANE273 element was used to mesh the SMA component of the composite system while the PLANE183 element was employed for the matrix. The two components were glued to each other in order to simulate perfect adhesion and were assigned with the same Poisson's ratio in order to eliminate any stiffening effects between the two components. A quadratic, 8-noded element mesh with a sizing of $h_{SMA}/4$ was chosen for both components of the composite, following convergence tests, and the simulations were conducted under plane-stress conditions.

ACCEPTED MANUSCRIPT

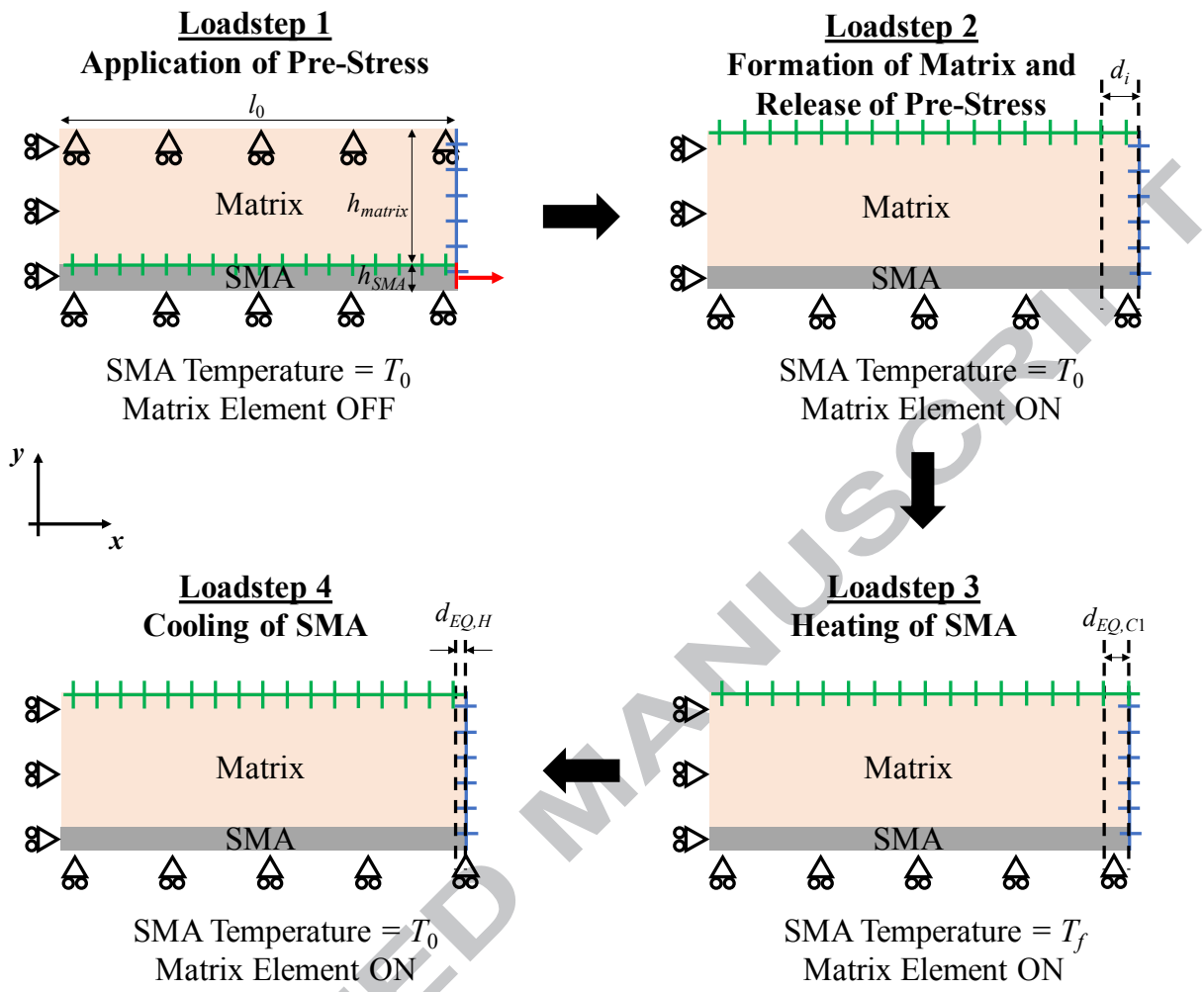

Figure 4: Diagram showing a schematic of the four-step FE simulation methodology used to model the SMA-matrix actuators. Note that each diagram depicts the initial state of the system before the loadstep begins. The rollers depict fixes of the node displacements in the *x*- and *y*-directions, while the green and blue crosses denote nodes with coupled displacements constraining them to remain aligned with the *x*- and *y*-axes respectively. The red line and arrow in Loadstep 1 indicate nodes which have been subjected to force-loading in the *x*-direction.

As shown in **Figure 4**, the initial geometry of the actuator composite was defined by the following parameters, l_0, the length of the actuator, h_{SMA}, the height of the SMA component and h_{matrix}, the height of the matrix. Since the matrix was assumed to possess linear elastic behaviour, the material properties of the matrix were defined through the linear Young's modulus, E_{matrix}, and the Poisson's ratio, v_{matrix}. In the case of the SMA component, the material properties were simulated using the Souza-Auricchio Shape Memory model [34][35]. The material properties were defined by the following parameters: the Poisson's ratio, v_{SMA}, the austenitic Young's modulus, E_A, the detwinned martensitic Young's modulus, E_{DM}, the hardening parameter, H, the elastic limit, R, the maximum transformation strain, e_L, the reference conversion temperature, T_0, and the temperature scaling parameter, β [36].

The simulations were conducted in four sequential steps as shown in **Figure 4**. In the first loadstep, after the system is constructed, the matrix elements are switched off using the Element Death option. This means that these elements may deform without undergoing stress

ACCEPTED MANUSCRIPT

and thus upon applying a force load, F_i, on the edge nodes of the SMA wire (see **Figure 4** – Loadstep 1), the entire stress of force loading is absorbed by the SMA. This means that in the first loadstep, essentially only the SMA component is loaded. In order to ensure that the entire system retains its rectangular shape, roller displacement fixes are applied on the bottom and left nodes of the composite and the nodes on the right edge are coupled and forced to remain aligned with the *y*-axis. The upper nodes of the SMA component are also coupled and constrained to remain aligned with the *x*-axis at all times during this loadstep, while the upper nodes of the matrix are constrained through roller displacements to remain fixed at their initial *y*-position of $h_{matrix}+h_{SMA}$. The latter constraint is necessary in order to ensure that the matrix retains more or less its original geometry during the first loadstep. These boundary conditions allow us to simulate the application of a uniaxial pre-stretch to the SMA component of the system before the introduction of the counterbalance component (see **Figure 1**), which in this case is the matrix.

In the second loadstep, the matrix element is switched on using the Element Birth option and the force load is set to zero. This simulates the formation of the matrix around the pre-stretched SMA component, as if a liquid matrix was poured on an SMA component in a mold. The constraints on the upper surface nodes of the SMA wire were removed and the roller fixes on the upper nodes of the matrix were replaced by coupling boundary conditions as shown in **Figure 4**. In the third loadstep, the SMA wire is heated to a higher temperature T_f, which is sufficient to ensure a complete austenitic transformation. Finally, in the fourth and final loadstep, the SMA component is re-cooled back to its initial temperature, T_0. For the last two steps, the heat distribution throughout the SMA component was uniform throughout, thus simulating the process of heating the SMA through the application of an electric current.

The following material properties were used to simulate the SMA: $v_{SMA} = 0.33$, $E_A = 70$ GPa, $H = 0.5$ GPa, $E_{DM} = 70$ GPa, $R = 45$ MPa, $e_L = 0.03$, $T_0 = 253.15$ K and $\beta = 7.5$ MPa K^{-1}. These material properties were taken from [35] and represent the material properties of a Nitinol SMA wire tested by [37]. The geometric parameters of the composite actuator and Poisson's ratio of the matrix were also kept constant with $v_{matrix} = 0.33$, $l_0 = 10$ mm, $h_{matrix} = 1.5$ mm and $h_{SMA} = 0.150$ mm. In order to vary the stiffness of the matrix, a range of Young's moduli, E_{matrix}, were used: 107 MPa, 214 MPa, 428 MPa, 856 MPa, 1,712 MPa, 3,424 MPa and 6,848 MPa, while various degrees of pre-stretch equivalent to a pre-strain, ε_i, of 2%, 3%, 4%, 5% and 6% were applied to SMA wire in Loadstep 1. Finally, in order to further test the robustness of the model, following these simulations a number of additional hypothetical cases where the SMA material parameter E_{DM} was greater or less than E_A were also simulated.

4. Results and Discussion

Before comparing the theoretical approach with the Finite Element model, the terms used in **Eq. 1-21** must be reparametrized in terms of the stress-strain behaviour of the SMA as predicted by the Souza-Auricchio model, the mechanical properties of the matrix and geometric parameters of the actuator composite. **Figure 5** shows the stress-strain plots which may be obtained for the material parameters listed in the previous section for the SMA at low martensite temperature, $T = 253.15$ K, and high austenite temperature, $T = 303.15$ K.

ACCEPTED MANUSCRIPT

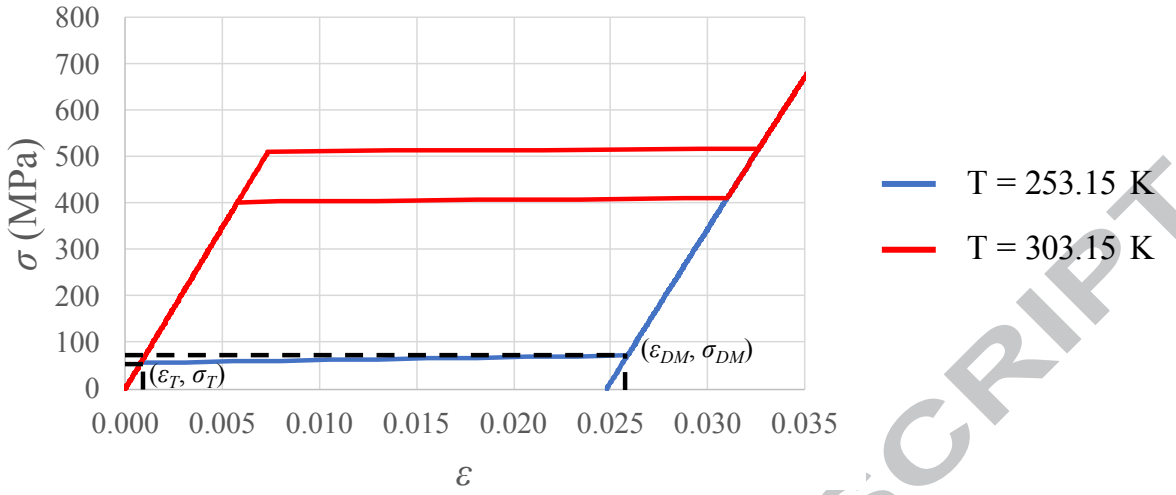

Figure 5: Plot showing the stress-strain curves obtained from the Souza-Auricchio model for loading followed by unloading of an SMA wire with the material parameters used here. The blue line is the martensitic SMA, while the red line is the austenitic SMA. Note that while austenitic SMA shows superelastic behaviour by recovering all its strain upon unloading and returning back to its original size, the martensitic SMA does not and on unloading returns to a strain value of *ca.* 0.025.

As shown in **Figure 5**, one may obtain the first and second step transformation points (ε_T, σ_T) and (ε_{DM}, σ_{DM}) respectively from this plot. These parameters may be used to define the parameters d_T, F_T, d_{DM} and F_{DM} as follows:

$$d_T = \varepsilon_T l_0 \qquad \textbf{Eq. 22}$$

$$d_{DM} = \varepsilon_{DM} l_0 \qquad \textbf{Eq. 23}$$

$$F_T = \sigma_T h_{SMA} \qquad \textbf{Eq. 24}$$

$$F_{DM} = \sigma_{DM} h_{SMA} \qquad \textbf{Eq. 25}$$

Since unit thickness is assumed for the FE simulation, the cross-sectional area of the SMA component is equal to h_{SMA}. The same holds true for the matrix, where the cross-sectional area is equal to h_{matrix}. The stiffnesses of the various martensitic phases, the austenitic phase and the matrix may also be rewritten in terms of the geometric parameters of the system (h_{SMA}, h_{matrix}, l_0), Young's moduli (E_M, E_T, E_{DM}, E_A) and applied pre-strain (ε_i) as:

$$k_M = \frac{E_M h_{SMA}}{l_0} \qquad \textbf{Eq. 26}$$

$$k_T = \frac{E_T h_{SMA}}{l_0} \qquad \textbf{Eq. 27}$$

$$k_{DM} = \frac{E_{DM} h_{SMA}}{l_0} \qquad \textbf{Eq. 28}$$

ACCEPTED MANUSCRIPT

$$k_A = \frac{E_A h_{SMA}}{l_0} \quad \textbf{Eq. 29}$$

$$k_{CB} = \frac{E_{matrix} h_{matrix}}{l_0 (\varepsilon_i + 1)} \quad \textbf{Eq. 30}$$

Note that the initial length of the matrix is dependent on the pre-strain applied to the SMA wire since it is formed around the pre-stretched SMA. By substituting these terms into **Eq. 1-21**, one may obtain the actuation and recovery displacements and forces of the simulated system through the analytical model. The extracted parameters from the plots shown in **Figure 5** were $\varepsilon_T = 0.000786$, $\sigma_T = 55.0000$ MPa, $\varepsilon_{DM} = 0.025874$, $\sigma_{DM} = 71.5078$ MPa and $E_T = 665$ MPa. E_A and E_{DM} were defined directly by the model parameters and since the Souza-Auricchio model allows for only one Young's modulus to represent the first linear phase of the stress-strain graph, E_M is equal to E_A.

Figure 6 shows the percentage actuation and recovery strokes obtained from the analytical model and the Finite Element simulations using these parameters. Percentage actuation stroke is defined as the percentage of actuation stroke or displacement relative to the initial length of the actuator as shown in **Eq. 31** while percentage recovery is defined as the percentage of recovery stroke relative to actuation stroke as shown in **Eq. 32**.

$$\%\text{Actuation Stroke} = \frac{d_A}{l_0} 100 \quad \textbf{Eq. 31}$$

$$\%\text{Recovery Stroke} = \frac{d_R}{d_A} 100 \quad \textbf{Eq. 32}$$

ACCEPTED MANUSCRIPT

ACCEPTED MANUSCRIPT

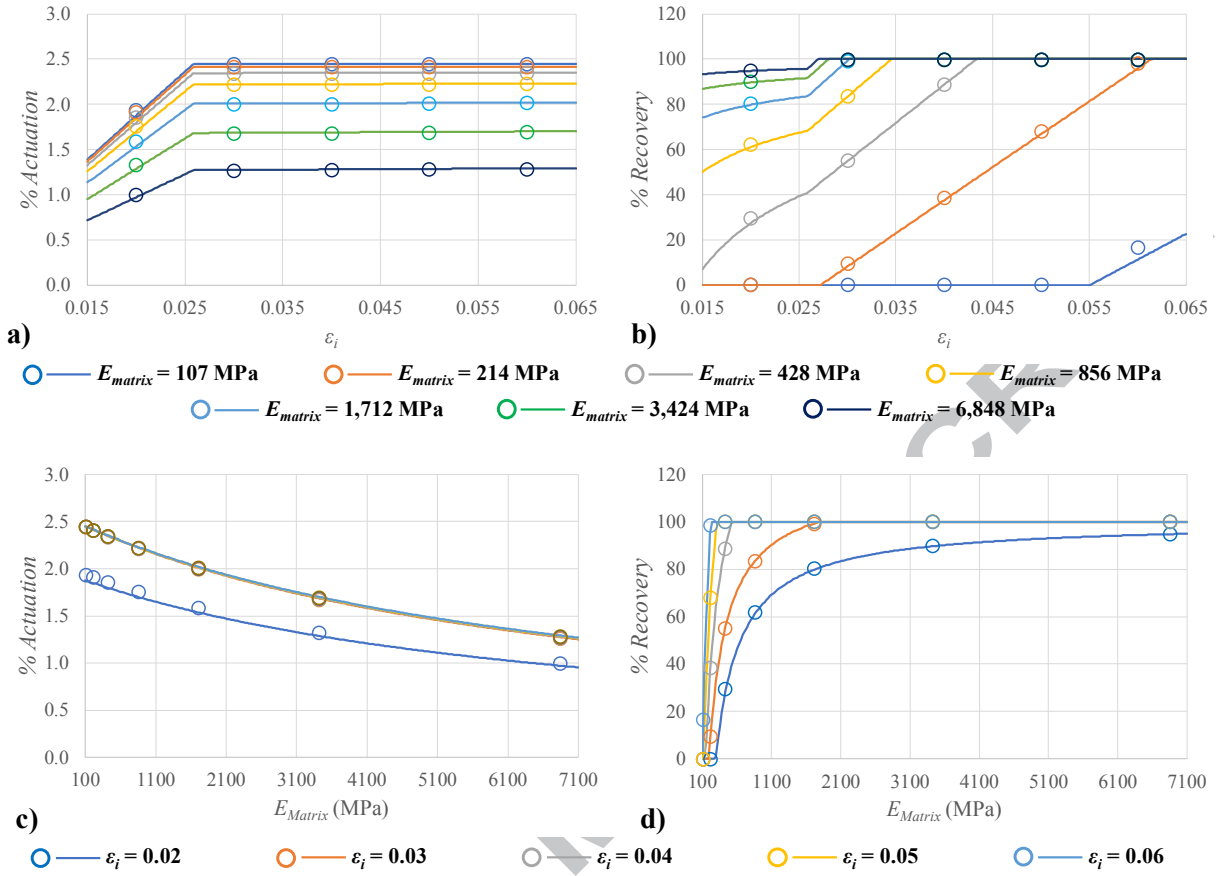

Figure 6: Plots showing the predicted percentage actuation stroke and recovery obtained from the analytical model (solid lines) and FE simulations (circles) against pre-strain, ε_i, and matrix Young's modulus, E_{matrix}.

As one may observe from **Figure 6**, the analytical and finite element results show very good agreement with each other indicating that the analytical expression can be used to obtain an accurate prediction of the actuation properties of an SMA composite actuator. The plots also highlight a number of distinct trends. For example, as shown in **Figure 6a**, the lower the matrix Young's modulus, and by extension the matrix stiffness, the greater the actuation percentage obtained. However, this increased actuation appears to come at the cost of recovery in some cases since as shown in **Figure 6b**, the actuator systems with the lowest counterbalance stiffness actually possess the lowest recovery percentages, with the most extreme cases showing a value of zero. The plot of percentage actuation stroke against pre-strain (see **Figure 6a**) also appears to be divided into two distinct regions. In the region where ε_i is below 0.0258, i.e. ε_{DM}, the extent of actuation is dependent on the amount of pre-strain applied to the SMA component. However, upon reaching this point the actuation stroke stops increasing with increasing pre-strain and stabilizes at a threshold value depending on the stiffness of the counterbalance component (see **Figure 6a,c**). The latter behaviour arises due to the fact that since E_A and E_{DM} are equal in this case, then by extension, k_A and k_{DM} are also identical and since **Eq. 3** and **Eq. 4** are expressed independently of d_i, the distance between $d_{EQ,C1}$ and $d_{EQ,H}$ remains constant irrespective of the pre-strain value. However, at pre-strain values below ε_{DM}, **Eq. 3** is exchanged with **Eq. 18**, which includes the variable d_i, due to the system still being in

ACCEPTED MANUSCRIPT

the transition phase upon forming the matrix and, hence, the actuation stroke of the system is dependent on the level of applied pre-strain.

A similar effect is observed for the plots of the percentage recovery. As one may observe from **Figure 6b**, these plots are divided into three distinct regions. The first non-linear region ends at a pre-strain value of ε_{DM} and is observed for similar reasons mention for the calculation of the percentage actuation. The second, linear part indicates the region where the system is pre-strained to higher values than ε_{DM} but $\varepsilon_{EQ,C1}$, the initial equilibrium strain of the system, is lower than ε_{DM}. This results in a case similar to the scenario shown in **Figure 3a**, where **Eq. 15** is required to calculate the cooling equilibration point due to the fact that the system recovers in the transition region of the SMA force-displacement plot. This is the case for all systems which show a recovery percentage value between 0% and 100%, including the systems which have a pre-strain value less than ε_{DM}. On the other hand, systems which possess a recovery percentage of zero possess an $\varepsilon_{EQ,C2}$, i.e. cooling equilibration point strain, value lower than ε_T, which, since E_A is equal to E_M, results in $d_{EQ,C2}$ as calculated from **Eq. 13** being equal to $d_{EQ,H}$, which results in a recovery stroke of zero. Finally if, $\varepsilon_{EQ,C1}$ is greater than ε_{DM}, then as indicated previously in the theoretical approach section, $\varepsilon_{EQ,C1} = \varepsilon_{EQ,C2}$ and thus a full recovery is obtained. As shown in **Figure 6b,d**, the latter cases are more prevalent when the matrix has a high stiffness value.

In all the cases shown in **Figure 6**, only the matrix stiffness and amount of pre-stress were altered with the material properties of the SMA wire remaining unchanged. However, although in the case study discussed above, the detwinned martensite and austenite Young's moduli, E_{DM} and E_A, were set to an equal value of 70 GPa, a number of experimental stress-strain plots of SMA wires found in literature indicate that this is not always the case. In view of this, in order to further validate the analytical model and analyse the effect of changing this parameter on the actuation properties of the entire composite system, an additional set of results where all the SMA and matrix material properties (including E_{matrix}, which was set to 856 MPa) and geometric parameters of the systems save for E_{DM} remained unchanged, were run. The results of these simulations are shown in **Figure 7a**.

ACCEPTED MANUSCRIPT

ACCEPTED MANUSCRIPT

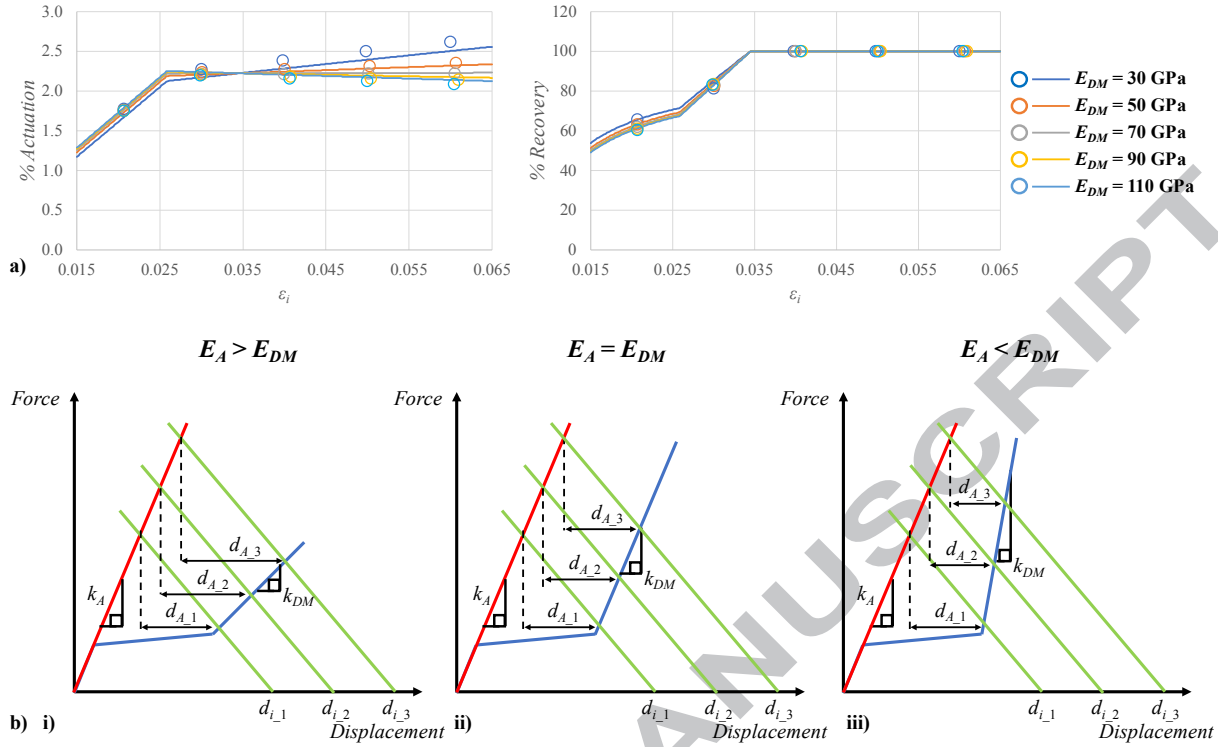

Figure 7: a) Plots showing the trends obtained through Finite Element modelling (circles) and the analytical model (lines) of %Actuation and %Recovery vs pre-strain, ε_i, for different E_{DM} values (E_A was constant at 70 GPa throughout). b) Qualitative force-displacement graphs explaining how the obtained actuation (d_A) changes with respect to the relative values of E_A and E_{DM}. Note that while in each case $d_{i\_1} < d_{i\_2} < d_{i\_3}$, in case i) when $E_A > E_{DM}$, $d_{A\_1} < d_{A\_2} < d_{A\_3}$, in case ii) where $E_A = E_{DM}$, $d_{A\_1} = d_{A\_2} = d_{A\_3}$, and finally in case iii) where $E_A < E_{DM}$, $d_{A\_1} > d_{A\_2} > d_{A\_3}$.

Again, the finite element and analytical model results show excellent agreement. As one may observe from the plots in **Figure 7a**, once $E_A \neq E_{DM}$, the level of pre-strain applied to the SMA component plays a vital role in determining the degree of actuation stroke, even if ε_i is greater than ε_{DM}, which was not the case in the previous set of results. On the other hand, the trends for the recovery are relatively unaffected. If $E_A < E_{DM}$, the extent of actuation stroke decreases with increasing strain while the contrary occurs if $E_A > E_{DM}$. These opposing trends occur due to the differences in k_A and k_{DM} values and are illustrated very clearly in the qualitative force-displacement plots shown in **Figure 7b**. The latter case is especially of interest since it indicates that by combining the SMA component with a counterbalance component one may actually obtain an enhanced resultant actuation stroke from the two-component composite actuator in comparison to the SMA component on its own. Intriguingly enough, a number of experimental tests on SMAs found in literature [38–40] indicate that while cases where $E_A < E_{DM}$ are relatively rare, SMAs which possess an E_A value greater or equal to E_{DM} are much more commonly found. This opens up a number of exciting possibilities for the design of SMA-based actuators since it indicates that the extent of actuation stroke may be controlled by the amount of pre-stretch applied to the SMA component, thus allowing a great deal of flexibility for designing a system with a desired actuation effect. However, here it is imperative to note that although one may use the analytical model presented to obtain a tailored actuation stroke and force, these two parameters are interdependent on each other and thus if one wishes to

ACCEPTED MANUSCRIPT

design an actuator with a desired stroke, then the magnitude of the actuation output force of the system is imposed by this parameter and *vice-versa*.

At this point, it is important to mention once again the fact that the analytical model presented here is based on the premise that a complete transformation from transition phase or detwinned martensite to austenite occurs upon heating. It is well known [41][42] that the transformation temperature, T_{Trans}, increases from the reference temperature, T_0, upon increasing stress within the SMA component and thus the greater the applied equilibrium point stress and strain ($\varepsilon_{EQ,C1}$, $\sigma_{EQ,C1}$,), the greater the temperature increase required to achieve complete austenitic transformation. In fact, **Figure 8** shows how T_{Trans} increased upon increasing $\varepsilon_{EQ,C1}$ for the various FE simulations shown in **Figure 6**. This should not be considered to be a very problematic issue when using many commercially available SMAs since when heating them through the application of an electric current [6,43] or any other quick-heating method, the change in temperature typically exceeds by far the temperature rise required to achieve complete austenitic transformation. However, it could be problem when very large pre-stretch values are applied to the SMA component, especially if the material properties of the SMA dictate that the transition temperature changes greatly with stress, and thus its effect should not be completely discounted in these cases. In addition, it must be mentioned that the model covers only the application of a uniaxial tensile pre-stretch of the SMA component and does not consider off-axis or multiaxial stretching, which is expected to result in a different force-displacement profile for the SMA component. While these conditions are not applicable to the most commonly used SMA geometries in actuators, i.e. wires and springs, they could be significant in certain niche applications involving, for example, SMA strips and thus it would be of interest to consider these effects in future studies.

Another key assumption of this model is that the effect of the application of pre-stretch on the SMA component is completely reversible, i.e. the SMA does not undergo failure or any other unrecoverable effects as a result of the applied initial loading which could affect its deformation behaviour. This condition depends strongly on the fatigue behaviour of the SMAs [44,45]. This means that the model also cannot be used to predict the effect of texture changes and other history-dependent changes [46,47] on the force-displacement profile of the SMA component. Finally, it is important to note that while both the Souza-Auricchio model and the analytical model presented here approximate the stress-strain behaviour of the SMA component in the form of linear plots, in reality experimental force-displacement plots are never strictly linear and thus the accuracy of the actuation and recovery predictions of both these approaches are entirely dependent on the goodness of the fit. Here it is also apt to mention that the approximation of the SMA force-displacement behaviour in the form of three linear plots presented here holds true primarily in the case of geometries such as wires, strips and springs which have a linear geometric stress-strain profile as is the case for the majority of SMA-based composite actuators. In the case of complex geometries or designs which possess non-linear force-displacement behaviour, the stress-strain approximation of the SMA component must be adjusted accordingly. In every case the design of the actuators is based on the complete knowledge of the force displacement plot of the SMA element both in fully martensitic and fully austenitic regime, which can be easily obtained experimentally.

ACCEPTED MANUSCRIPT

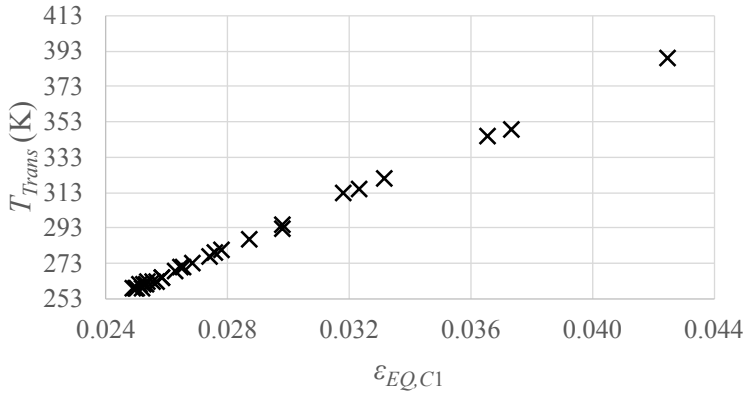

Figure 8: Plot showing how T_{Trans} changes from the original reference temperature, T_0 = 253.15 K, upon increasing the first equilibrium point strain for the FE simulations presented in Figure 6.

Despite these limitations, the analytical model presented here provides a simple, yet effective method through which one may design a SMA composite actuator with a tailored actuation and recovery stroke based off the individual force-displacement or stress-strain behaviour of the two components. The model may be used for a quite straightforward design of a desired actuator through the correct definition of two main design parameters which may be easily varied according to necessity, i.e. the initial applied prestrain, d_i, and the stiffness of the counterbalance component, k_{CB}. The model has been shown to be extremely robust and was validated using FE simulations based on the well-established Souza-Auricchio shape memory numerical model. In the SMA wire/matrix composite example presented in this work, the matrix, which acts as the counterbalance component of the actuator, was assumed to possess a linear elastic behaviour for the sake of simplicity. However, the same principles applied to derive this analytical model could also be used to predict the behaviour of a counterbalance component which possess hyperelastic behaviour or any other nonlinear behaviour as well. In this case one may replace **Eq. 5** with the nonlinear counterbalance equation and reparametrize the model accordingly. However, in its current state, the model does not cater for cases involving an SMA geometry which possesses a non-uniform stress gradient during deformation where the three distinct stages of martensite stress-strain behaviour become intertwined. Further improvements and modifications to the model, which could be covered in future studies, must be conducted before this may be achieved. In addition, while in the FE simulations the stiffness of the matrix was altered by changing the Young's modulus of the matrix (which was done for the sake of computational efficiency), the model shows how the same effect could also be obtained by changing the cross-sectional area of the matrix, which is more easily achieved for practical applications. Moreover, despite the fact that the SMA component used for the numerical validation had a very low actuation stroke (the initial linear martensite region extends only up to *ca.* 0.0008 strain, ε_T, and ε_{DM} is equal to 0.0258), a number of high strain SMA wires and springs have been shown to possess much higher actuation strokes, which means that by changing the geometric parameters of the system one may be able to have a greater degree of flexibility in obtaining a tailored stroke output.

5. Conclusion

ACCEPTED MANUSCRIPT

In this work we have presented an analytical model which may be used to predict the actuation stroke and recovery of an SMA composite actuator. This model is expected to be of significant aid in the development of these actuators, particularly at the pre-design stage where the model could be used to elucidate the desired stiffness of the counterbalance element, through material properties and geometric parameters, and to find the ideal pre-stretch value for the SMA component. This method was validated using FE simulations where an SMA composite actuator system was modelled in the form of a 2D SMA strip/wire embedded within an elastic matrix. The results obtained from the FE simulations and the analytical predictions of the derived model showed extremely good agreement and allowed for a thorough investigation of the various trends which may be obtained by changing a number of material and geometric parameters such as level of pre-stretch, matrix stiffness and relative Young's moduli of the different phases of the SMA component. It is envisaged that the work presented here will prove to be of considerable help for the design of SMA-based actuators in the future and it is hoped that our findings will advance and stimulate further interest in this exciting field of study.

Acknowledgements

This work was partially supported by MIUR with project Prin 2015 n. 2015RT8Y45-PE8 on Smart Composite Laminates.

Data Availability

The raw/processed data required to reproduce these findings cannot be shared at this time as the data also forms part of an ongoing study.

References

[1] Funakubo. Shape Memory Alloys. Boca Raton, Florida, USA: CRC Press - Boca Raton, Florida, USA; 1987.

[2] Lagoudas DC. Shape Memory Alloys. vol. 1. Boston, MA: Springer US; 2008. doi:10.1007/978-0-387-47685-8.

[3] Spaggiari A, Castagnetti D, Golinelli N, Dragoni E, Scire Mammano G. Smart materials: Properties, design and mechatronic applications. Proc Inst Mech Eng Part L J Mater Des Appl 2016;0:1–29. doi:10.1177/1464420716673671.

[4] Mohd Jani J, Leary M, Subic A, Gibson MA. A review of shape memory alloy research, applications and opportunities. Mater Des 2014;56:1078–113. doi:10.1016/j.matdes.2013.11.084.

[5] Bodaghi M, Damanpack AR, Aghdam MM, Shakeri M. A robust three-dimensional phenomenological model for polycrystalline SMAs: Analytical closed-form solutions. Int J Eng Sci 2014;82:1–21. doi:10.1016/j.ijengsci.2014.05.002.

[6] Sun L, Huang WM, Ding Z, Zhao Y, Wang CC, Purnawali H, et al. Stimulus-responsive shape memory materials: A review. Mater Des 2012;33:577–640. doi:10.1016/j.matdes.2011.04.065.

ACCEPTED MANUSCRIPT

[7] Petrini L, Migliavacca F. Biomedical Applications of Shape Memory Alloys. J Metall 2011;2011:1–15. doi:10.1155/2011/501483.

[8] Migliavacca F, Petrini L, Massarotti P, Schievano S, Auricchio F, Dubini G. Stainless and shape memory alloy coronary stents: A computational study on the interaction with the vascular wall. Biomech Model Mechanobiol 2004;2:205–17. doi:10.1007/S10237-004-0039-6.

[9] Kuribayashi K, Tsuchiya K, You Z, Tomus D, Umemoto M, Ito T, et al. Self-deployable origami stent grafts as a biomedical application of Ni-rich TiNi shape memory alloy foil. Mater Sci Eng A 2006;419:131–7. doi:10.1016/j.msea.2005.12.016.

[10] Song C. History and Current Situation of Shape Memory Alloys Devices for Minimally Invasive Surgery. Open Med Devices J 2010;2:24–31. doi:10.2174/1875181401002020024.

[11] Oishi R, Nagai H. Strain sensors of shape memory alloys using acoustic emissions. Sensors Actuators, A Phys 2005;122:39–44. doi:10.1016/j.sna.2005.03.055.

[12] Ikuta K. Micro/miniature shape memory alloy actuator. Proceedings., IEEE Int. Conf. Robot. Autom., IEEE Comput. Soc. Press; 1990, p. 2156–61. doi:10.1109/ROBOT.1990.126323.

[13] Chiu JT, Shen CL. Analysis of the restitution characteristics of a golf ball colliding with a club-head. Jpn J Ind Appl Math 2005;22:429–42. doi:10.1007/BF03167493.

[14] Masters BP, van Schoor MC, Jessiman AW. Golf club shaft with Superelastic tensioning device. US 2003/0017884 A1, 2003. doi:10.1093/iwc/iwv022.

[15] Bodaghi M, Damanpack AR, Aghdam MM, Shakeri M. A phenomenological SMA model for combined axial-torsional proportional/non-proportional loading conditions. Mater Sci Eng A 2013;587:12–26. doi:10.1016/j.msea.2013.08.037.

[16] Asadi H, Bodaghi M, Shakeri M, Aghdam MM. Nonlinear dynamics of SMA-fiber-reinforced composite beams subjected to a primary/secondary-resonance excitation. Acta Mech 2014;226:437–55. doi:10.1007/s00707-014-1191-4.

[17] Bodaghi M, Shakeri M, Aghdam MM. Thermo-mechanical behavior of shape adaptive composite plates with surface-bonded shape memory alloy ribbons. Compos Struct 2015;119:115–33. doi:10.1016/j.compstruct.2014.08.027.

[18] Ishii H, Ting KL. SMA actuated compliant bistable mechanisms. Mechatronics 2004;14:421–37. doi:10.1016/S0957-4158(03)00068-0.

[19] Nespoli A, Besseghini S, Pittaccio S, Villa E, Viscuso S. The high potential of shape memory alloys in developing miniature mechanical devices: A review on shape memory alloy mini-actuators. Sensors Actuators, A Phys 2010;158:149–60. doi:10.1016/j.sna.2009.12.020.

[20] Spaggiari A, Mammano GS, Dragoni E, A. Spaggiari GSM and ED. Optimum Mechanical Design of Binary Actuators Based on Shape Memory Alloys. Chapter "Smart Actuation Sens Syst - Recent Adv Futur Challenges" Intech Publ 2012:3–34. doi:10.5772/2760.

[21] Reynaerts D, Van Brussel H. Design aspects of shape memory actuators. Mechatronics 1998;8:635–56. doi:10.1016/S0957-4158(98)00023-3.

ACCEPTED MANUSCRIPT

[22] Spinella I, Dragoni E. Design equations for binary shape memory actuators under dissipative forces. Proc Inst Mech Eng Part C J Mech Eng Sci 2009;223:531–43. doi:10.1243/09544062JMES1232.

[23] Spaggiari A, Dragoni E. Analytical and numerical modeling of shape memory alloy Negator springs for constant-force, long-stroke actuators. J Intell Mater Syst Struct 2013;25:1139–48. doi:10.1177/1045389X13493354.

[24] Scirè Mammano G, Dragoni E. Modeling of Wire-on-Drum Shape Memory Actuators for Linear and Rotary Motion. J Intell Mater Syst Struct 2011;22:1129–40. doi:10.1177/1045389X11411214.

[25] Spinella I, Scirè Mammano G, Dragoni E. Conceptual Design and Simulation of a Compact Shape Memory Actuator for Rotary Motion. J Mater Eng Perform 2009;18:638–48. doi:10.1007/s11665-009-9421-y.

[26] Scirè Mammano G, Dragoni E. Increasing stroke and output force of linear shape memory actuators by elastic compensation. Mechatronics 2011;21:570–80. doi:10.1016/j.mechatronics.2011.02.005.

[27] Cha S-W, Kang S-R, Hwang Y-H, Choi S-B. A single of MR sponge tactile sensor design for medical applications 2017;10164:101642D. doi:10.1117/12.2259769.

[28] Renata C, Huang WM, He LW, Yang JJ. Shape change/memory actuators based on shape memory materials. J Mech Sci Technol 2017;31:4863–73. doi:10.1007/s12206-017-0934-2.

[29] Bettini P, Riva M, Sala G, Di Landro L, Airoldi A, Cucco J. Carbon fiber reinforced smart laminates with embedded SMA actuators-part I: Embedding techniques and interface analysis. J Mater Eng Perform 2009;18:664–71. doi:10.1007/s11665-009-9384-z.

[30] Riva M, Bettini P, Di Landro L, Sala G, Airoldi A. Carbon fiber-reinforced smart laminates with embedded SMA actuators-part II: Numerical models and empirical correlations. J Mater Eng Perform 2009;18:672–8. doi:10.1007/s11665-009-9417-7.

[31] Simoneau C, Terriault P, Lacasse S, Brailovski V. Adaptive composite panel with embedded SMA actuators: Modeling and validation. Mech Based Des Struct Mach 2014;42:174–92. doi:10.1080/15397734.2013.864246.

[32] Kim SW, Koh JS, Cho M, Cho KJ. Design & analysis a flytrap robot using bi-stable composite. Proc - IEEE Int Conf Robot Autom 2011:215–20. doi:10.1109/ICRA.2011.5980318.

[33] Spaggiari A, Dragoni E. Analytical and numerical modeling of shape memory alloy Negator springs for constant-force, long-stroke actuators. J Intell Mater Syst Struct 2014;25:1139–48. doi:10.1177/1045389X13493354.

[34] Souza AC, Mamiya EN, Zouain N. Three-dimensional model for solids undergoing stress-induced phase transformations. Eur J Mech A/Solids 1998;17:789–806. doi:10.1016/S0997-7538(98)80005-3.

[35] Auricchio F, Petrini L. Improvements and algorithmical considerations on a recent three-dimensional model describing stress-induced solid phase transformations. Int J Numer Methods Eng 2002;55:1255–84. doi:10.1002/nme.619.

ACCEPTED MANUSCRIPT

[36] ANSYS16 n.d.

[37] Sittner P, Hara Y, Tokuda M. Experimental study on the thermoelastic martensitic transformation in shape memory alloy polycrystal induced by combined external forces. Metall Mater Trans A 1995;26:2923–35. doi:10.1007/BF02669649.

[38] Ng KL, Sun QP. Stress-induced phase transformation and detwinning in NiTi polycrystalline shape memory alloy tubes. Mech Mater 2006;38:41–56. doi:10.1016/j.mechmat.2005.05.008.

[39] Liu Y, Xie Z, Van Humbeeck J. Cyclic deformation of NiTi shape memory alloys. Mater Sci Eng A 1999;273–275:673–8. doi:10.1016/S0921-5093(99)00347-0.

[40] Nemat-Nasser S, Guo WG. Superelastic and cyclic response of NiTi SMA at various strain rates and temperatures. Mech Mater 2006;38:463–74. doi:10.1016/j.mechmat.2005.07.004.

[41] Auricchio F, Taylor R. Shape-memory alloys: modelling and numerical simulations of the finite-strain superelastic behavior. Comput Methods Appl Mech … 1997.

[42] Huang W. Modified Shape Memory Alloy (SMA) model for SMA wire based actuator design. J Intell Mater Syst Struct 1999;10:221–31.

[43] An L, Huang WM, Fu YQ, Guo NQ. A note on size effect in actuating NiTi shape memory alloys by electrical current. Mater Des 2008;29:1432–7. doi:10.1016/j.matdes.2007.09.001.

[44] Scirè Mammano G, Dragoni E. Functional fatigue of Ni-Ti shape memory wires under various loading conditions. Int J Fatigue 2014;69:71–83. doi:10.1016/j.ijfatigue.2012.03.004.

[45] Scirè Mammano G, Dragoni E. Effect of Stress, Heating Rate, and Degree of Transformation on the Functional Fatigue of Ni-Ti Shape Memory Wires. J Mater Eng Perform 2015;24:2709–19. doi:10.1007/s11665-015-1561-7.

[46] Gao XY, Huang WM. Transformation start stress in non-textured shape memory alloys. Smart Mater Struct 2002;11:256–68.

[47] Huang WM. Transformation progress in shape. Smart Mater Struct 2004;13:443–8. doi:10.1088/0964-1726/13/2/023.

ACCEPTED MANUSCRIPT